ECG Triggering in Ultra-High Field Cardiovascular MRI

Daniel Stäb[1,2], Juergen Roessler[3], Kieran O'Brien[4], Christian Hamilton-Craig[5], and Markus Barth[1]

[1]The Centre for Advanced Imaging, The University of Queensland, Brisbane, Queensland, Australia; [2]Department of Diagnostic and Interventional Radiology, University of Würzburg, Würzburg, Germany; [3]Siemens Healthcare GmbH, Erlangen, Germany; [4]Siemens Healthcare Pty Ltd, Brisbane, Australia; and [5]Richard Slaughter Centre of Excellence in CVMRI, The Prince Charles Hospital, Brisbane, Queensland, Australia

Corresponding Author:
Daniel Stäb
The Centre for Advanced Imaging,
The University of Queensland,
Brisbane St Lucia, QLD 4072, Australia;
E-mail: daniel.staeb@cai.uq.edu.au

Key Words: ECG, ultra-high field, magnetohydrodynamic effect, cardiac, MRI
Abbreviations: Magnetohydrodynamic (MHD), electrocardiogram (ECG), cardiovascular magnetic resonance (CMR), vectorcardiography (VCG)

ABSTRACT

Cardiac magnetic resonance imaging at ultra-high field ($B_0 \geq 7$ T) potentially provides improved resolution and new opportunities for tissue characterization. Although an accurate synchronization of the acquisition to the cardiac cycle is essential, electrocardiogram (ECG) triggering at ultra-high field can be significantly impacted by the magnetohydrodynamic (MHD) effect. Blood flow within a static magnetic field induces a voltage, which superimposes the ECG and often affects the recognition of the R-wave. The MHD effect scales with B_0 and is particularly pronounced at ultra-high field creating triggering-related image artifacts. Here, we investigated the performance of a conventional 3-lead ECG trigger device and a state-of-the-art trigger algorithm for cardiac ECG synchronization at 7 T. We show that by appropriate subject preparation and by including a learning phase for the R-wave detection outside of the magnetic field, reliable ECG triggering is feasible in healthy subjects at 7 T without additional equipment. Ultra-high field cardiac imaging was performed with the ECG signal and the trigger events recorded in 8 healthy subjects. Despite severe ECG signal distortions, synchronized imaging was successfully performed. Recorded ECG signals, vectorcardiograms, and large consistency in trigger event spacing indicate high accuracy for R-wave detection.

INTRODUCTION

Cardiovascular magnetic resonance (CMR) is an important and well-established clinical tool for the diagnosis and management of cardiovascular diseases, and it is the standard of reference for the evaluation of cardiac morphology and function (1-3). CMR must overcome the challenges introduced because of cardiac and respiratory motion. In the clinic, CMR relies on accurate cardiac gating alongside parallel imaging (4, 5), simultaneous multi-slice imaging (6-8), or other acceleration methods (9, 10) to address limitations due to motion. However, the fact remains that CMR must always make a tradeoff between spatiotemporal resolution and signal-to-noise ratio.

The signal-to-noise ratio gain inherent at higher field strengths (11) has recently led to an increased use of high field systems with $B_0 = 3$ T for clinical CMR (12), and moreover, it has encouraged investigations into ultra-high field ($B_0 \geq 7$ T) CMR (13-15). Apart from enabling spatial resolutions that exceed today's limits (16), CMR at ultra-high field offers new opportunities for magnetic resonance-based tissue characterization (17, 18) or metabolic imaging (19).

Cardiac gating is usually performed using electrocardiogram (ECG) triggering. In general, vectorcardiography (VCG)-based QRS detection algorithms (20) are used, which aim to detect the R-wave in their peak by recognizing the R-wave's rising edge. However, ECG signal distortions from several effects have been challenging at ultra-high field. The interaction of the conductive fluid blood with the static magnetic field B_0, for instance, induces a voltage perpendicular to B_0 and the direction of flow that superimposes on the ECG signal (21). This so-called magnetohydrodynamic (MHD) effect is particularly large during the early systolic phase, when the blood is ejected from the left ventricle into the aortic arch. Hence, it mainly affects the T-wave of the ECG signal (22-24). The probability that a rising edge of an MHD artifact is similar to the rising edge of the R-wave is generally nonzero. Consequently, deteriorated cardiac synchronization is likely in the presence of strong MHD artifacts that are similar to the R-wave's rising edge. Problems have been observed at clinical field strengths such as 3 T (25, 26), and because the MHD effect scales with B_0, distortions have been reported to be worse at ultra-high field (27-29). In addition, the time-varying magnetic gradient fields, which induce voltage perturbations in the ECG leads, also distort the ECG signal. To avoid motion artifacts, the lengthening of scan times and scan repetitions that result from poor ECG triggering, the establish-

ISSN 2379-1381 http://dx.doi.org/10.18383/j.tom.2016.00193

ment of a stable cardiac synchronization technique is essential to advance ultra-high field CMR.

Pulse triggering is often used in cases were the conventional ECG approach fails (26). However, being derived from softly shaped peaks in the pulse wave signal, the trigger events are subject to immanent enhanced jittering (28, 30), which commonly introduces trigger-related image artifacts. Because the trigger events are also delayed with respect to the R-wave, pulse triggering is unsuitable for modalities like myocardial tagging that require an accurate detection of the R-wave.

Doppler ultrasound (30) and acoustic trigger devices (28, 31) as well as self-navigation (32-34) and pilot tone navigation (35) have recently been explored as alternative tools to conventional ECG triggering. In addition, advanced ECG detection algorithms (36-40) have been proposed, and promising results have been shown in initial studies.

Here, we explore the technical capabilities of a 7 T research MRI system and state-of-the-art 3-lead ECG equipment for cardiac synchronization at ultra-high field. Our initial study shows that by including an appropriate ECG learning phase outside of the magnetic field, existing ECG trigger technology in 7 T research systems allows for generating stable and reliable ECG trigger signals.

METHODOLOGY

All measurements were performed on a noncommercial 7 T whole-body research MRI scanner (Siemens Healthcare GmbH, Erlangen, Germany) under institutional review board permission. The gradient system provided a maximum gradient strength of 70 mT/m and a slew rate of 200 T/m/s. A dedicated 7 T cardiac Tx/Rx array with 8 transmit and 32 receive channels (MRI Tools GmbH, Berlin, Germany) was used for radiofrequency transmission and signal reception. The coil array was operated in single-channel transmit mode. To improve the B_0 field homogeneity, third-order shimming was used. For all human in vivo experiments, written informed consent was obtained before the examination as approved by the local ethics committee.

Cardiac Synchronization

For cardiac synchronization, a 3-lead ECG trigger device (Siemens Healthcare GmbH, Erlangen, Germany) using wireless signaling was used in conjunction with the standard trigger algorithm provided by the device manufacturer. The basic properties of this algorithm are briefly described in the following paragraph. For a detailed description, we refer the interested reader to work by Frank et al. (41).

To ensure an accurate detection of the peak of the R-wave, the trigger algorithm learns the shape of the rising edge of the R-wave during an initial learning phase in both ECG channels. Learning is performed while the subject is lying on the patient table outside of the magnet bore, where the MHD effect is typically negligible.

Once learning is completed, the trigger algorithm continuously compares different derived entities (ie, derivatives, filtered versions of derivatives) [for details refer Frank et al.'s study (41)] of the incoming ECG signal with the corresponding entities of the learned shape in real time. The comparisons are mainly based on 2 filter functions. The first is a matched filter, which is widely used in telecommunications (42) and mathematically corresponds to forming the correlation of the 2 signals. The filter function is given by the following equation:

$$m_j(\tau) = a_j \cdot \sum_{i=0}^{\Delta t} s_j(\tau - \Delta t + t) \cdot r_j^*(t), \qquad (1)$$

where a is a normalization factor, Δt depicts the period of comparison, and j refers to the signal entity for comparison. The incoming and the reference signal entities are depicted by $s(t)$ and $r(t)$, respectively. Both signal entities are complex with the real and imaginary components derived from the 2 ECG channels. The second filter function sums up the squared differences between the incoming ECG signal and the learned signal shape according to the following equation:

$$q_j(\tau) = b_j \cdot \sum_{t=0}^{\Delta t} (|s_j(\tau - \Delta t + t) \cdot r_j(t)|)^2 \qquad (2)$$

with b accounting for normalization. Trigger events are initiated by thresholding the filtered signals, m_j and q_j. In addition to using those filters, the angle of the VCG vector, which is spanned by the signal in the 2 ECG channels at each time instant, is used for R-wave detection. This angle criterion is implemented as a necessary, but not sufficient, condition for a trigger generation. The trigger algorithm showed an overall high performance at 1.5 T (43).

In Vivo Measurements

To evaluate the performance of the underlying ECG trigger algorithm, cardiac cine imaging at ultra-high field was performed in 8 healthy volunteers. Before starting the imaging procedure, ECG electrodes were placed onto the chest of the subject, following the instructions of the trigger device manufacturer, and in conjunction with a senior electrophysiology cardiac scientist. In 2 volunteers, the chest hair was removed in the target area before electrode placement to ensure good coupling at the body/electrode interface. After positioning the subject on the patient table, the ECG trigger device leads were connected to the electrodes, which automatically started the learning phase of the ECG algorithm. A pulse sensor (Siemens Healthcare GmbH, Erlangen, Germany) was attached to the subject's index finger as a backup trigger device. After finishing all other preparatory steps, the learning phase of the ECG algorithm was stopped to initiate the R-wave detection mechanism. The signals detected in both available ECG channels and the generated trigger events were recorded throughout all examinations.

Cardiac cine imaging was performed using a high-resolution breath-held ECG retro-gated segmented 2-dimensional spoiled gradient echo (FLASH) sequence with the following acquisition parameters: field of view = 360 × 270 (360 × 338) mm^2, matrix = 256 × 192 (256 × 240), slice thickness = 4.0 mm, echo time = 3.13 milliseconds, repetition time = 6.1 milliseconds, receiver bandwidth = 592 Hz/px, flip angle = 60°, phases = 20, segments = 7, and temporal resolution = 43 milliseconds. Parallel imaging was used with an acceleration factor of R = 2. All images were reconstructed online using GRAPPA with 34 reference lines for weight set calculation.

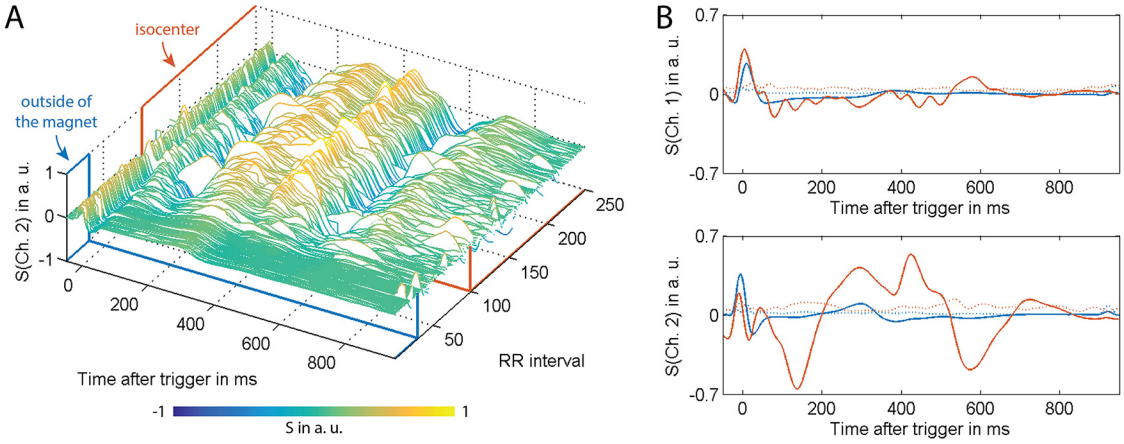

Figure 1. Electrocardiogram (ECG) signal time curves obtained in a healthy subject. Evolution of the ECG signal in channel 2 across consecutive RR-intervals during the transition from outside into the isocenter of the magnet (A). All curves were aligned based on observed trigger events. RR-intervals recorded outside and at the isocenter of the magnet are marked by blue and red lines, respectively. During the transition into the magnet (RR-intervals 30–100), the magnetohydrodynamic (MHD) effect increasingly impacts the ECG signal. Signal time curves averaged over 40 consecutive RR-intervals (solid) and corresponding standard deviation (dotted) following alignment by the observed trigger events observed outside (blue) and at the isocenter (red) of the magnet (B).

Qualitative Evaluations

The performance of the underlying trigger algorithm and the impact of the MHD effect onto the performance was qualitatively evaluated based on the recorded ECG signals. Signal time curves for the individual ECG channels were visually assessed. VCG plots were generated and examined to identify mistriggering. Finally, the time intervals between succeeding trigger events were analyzed to obtain an estimate on the amount of false positive and false negative trigger events.

RESULTS

A general overview of the MHD effect at ultra-high field can be gained from Figure 1A. It shows the change of the detected signal in one of the 2 ECG channels over several RR-intervals during the transition of the examined subject into the isocenter of the magnet. Outside of the magnet bore, the signal is generally smooth and undistorted, and the R-wave is easy to distinguish as the highest peak. With increasing magnetic flux density, the MHD-related alterations of the ECG become increasingly pronounced and result in a significant distortion of the ECG signal at the magnet's isocenter. In the depicted case, the distorted T-wave clearly exceeds the R-wave.

Individual ECG channels can be affected in different ways, as shown in Figure 1B, which compares the MHD effect on the signals of the 2 different ECG channels. To reduce the influence of inter-RR signal fluctuations, the ECG signals were averaged over 40 consecutive RR-intervals. The signals detected in both channels experience distortions at the isocenter of the magnet. However, only in channel 2 does the overall shape of the signal considerably change, and the R-wave is exceeded by the distorted ECG segments. Despite the significant impact of the MHD effect, the QRS complex is clearly identifiable in both channels and—as can be seen from the accurate alignment of the individual RR-intervals—has been accurately detected by the trigger algorithm for each of the displayed cardiac cycles.

Exemplary VCG plots obtained in 3 volunteers outside and at the isocenter of the magnet are given in Figure 2. In each vectorcardiogram, the ECG signal recorded in channel 2 is plotted against the signal measured in channel 1 over several RR-intervals. Associated trigger events are superimposed (black circles). The data were collected outside of the magnet bore (first row, blue), at the isocenter in the absence of gradient activity during free breathing (second row, red) and during a breath-held cine scan (third row, yellow). The MHD effect-related increase of the ECG signal variations within each RR-interval is apparent when comparing the vectorcardiograms obtained outside and inside of the magnet. In addition, the large magnetic field introduces considerable changes in the shape of the vectorcardiograms. Alterations can also be observed, when comparing data collected during free breathing and breath-hold periods. The characteristic VCG curves including the trigger events tend to be dispersed along the vertical axis, when obtained during free breathing (second row). As depicted by the enlarged section in Figure 2C (third row), gradient activity seems to introduce only tiny additional deflections in the VCG signal. For each subject, the location of the trigger events in the VCG plots is preserved in the vast majority of cases when exposing the subject to the ultra-high static magnetic field and dynamic gradient fields.

The accuracy of the trigger algorithm is shown in more detail in Figure 3. For one of the volunteers, ECG signal curves obtained outside of the magnet bore (Figure 3A) and at the magnet's isocenter (Figure 3, B and C) are compared with each other. The MHD effect-related distortions of the ECG signal are clearly recognizable. Despite these distortions, trigger events are typically placed accurately. Only on rare occasions, false nega-

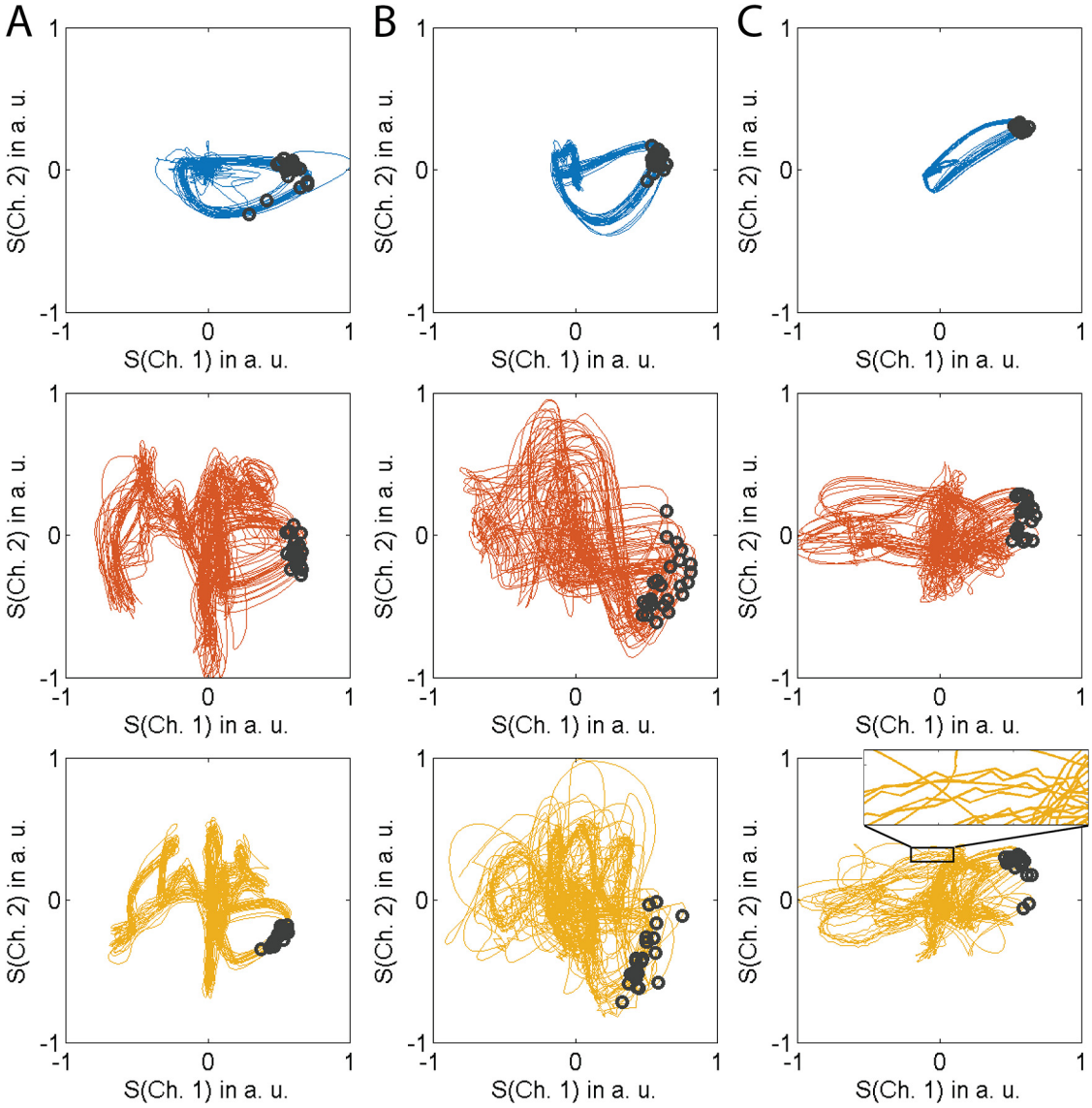

Figure 2. Vectorcardiograms obtained in 3 healthy subjects outside of the magnet (first row, blue), at the isocenter of the magnet during free breathing (second row, red), and during a breath-held cine acquisition (third row, yellow), each within a time-frame of 20 seconds (A–C). The depicted scales reflect the actual relative signal amplitudes between the channels. The generally small high-frequency signal variations induced by the imaging gradients can be seen in the enlarged section in the third row for subject (C).

tive and misplaced trigger events were observed. False positive events were extremely rare. This is the case even in presence of severe additional distortions (Figure 3C), which, in this case, can be attributed to enhanced inhaling and exhaling in preparation of a scan-related breath-hold. As seen in the enlarged section, the gradient activity of the scan causes smaller variations of the ECG signal. The start of the scan is marked by the dashed line.

An impression of the high trigger accuracy can also be gained from Figure 4, which depicts histograms of the time intervals between consecutive trigger events in 3 healthy subjects. While the width of the histogram peak reflects the variation of the subject's heart rate, outliers indicate false positive trigger events and undetected RR-intervals. The spacing between almost all trigger events is in the range of a single RR-interval. Only a few counts are spread out along the horizontal axis of the histogram.

ECG-triggered cardiac cine imaging worked generally well with the used synchronization setup. Representative examples of cardiac cine images obtained at 7 T are depicted in Figure 5. Shown are diastolic and systolic time frames of a short-axis (top row) and a 4-chamber long-axis view (bottom row) of a healthy subject's heart (see online Supplemental Video 1 PLAY VIDEO and Video 2 PLAY VIDEO). The myocardial walls are well delineated, and the images are free of visible artifacts that could be related to unsuccessful ECG triggering. The long-axis views show slight signal inhomogeneities introduced by

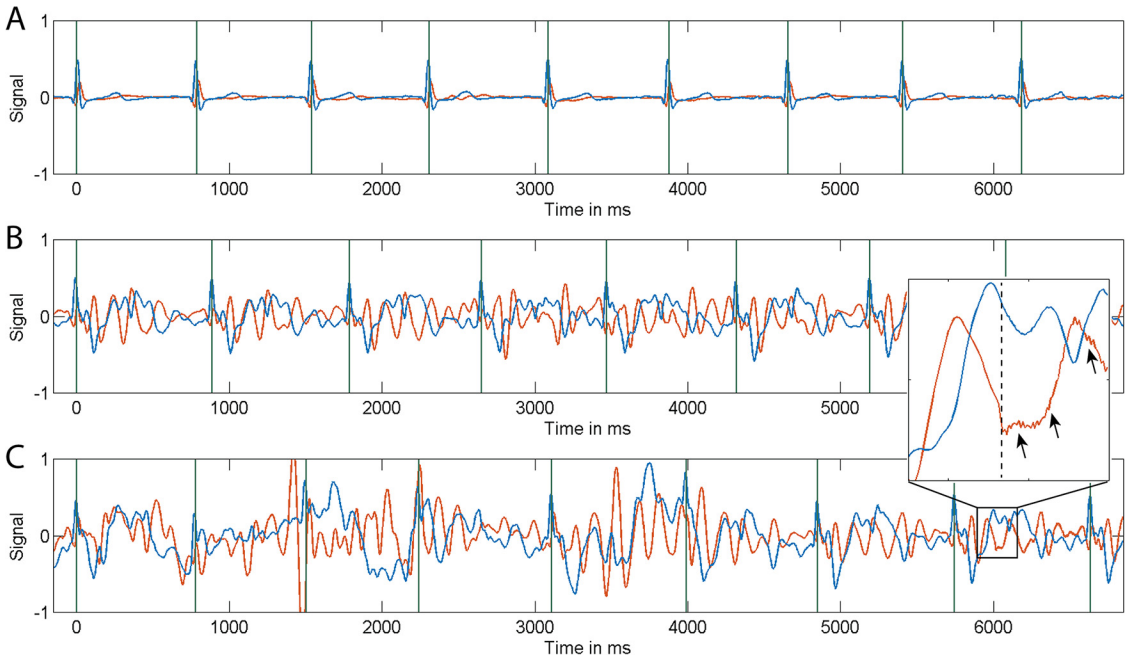

Figure 3. ECG signal over time measured in one of the volunteers outside of the magnet (A) and at the isocenter of the magnet (B–C) in the first (red) and second (blue) channel of the ECG. Trigger events (green vertical lines) are typically placed accurately at the peak of the R-wave. The larger distortions in (C) can be attributed to deep breathing preceding a breath-held cine acquisition. The enlarged section visualizes the start of the sequence (dashed line) and the effect of the imaging gradients on the ECG signal (arrows).

destructive B1 interferences (arrows). Moreover, flow effects are pronounced because of the high flip angle used.

DISCUSSION

For the medical application of CMR, the accurate synchronization of the imaging protocol to the cardiac cycle is essential to achieve high image quality and accurate results in functional evaluations. In this initial study, we explored the applicability of existing and state-of-the-art 3-lead ECG trigger technology for cardiac synchronization at the ultra-high field strength of 7 T. Without using additional hardware, the underlying trigger algorithm generated reliable ECG trigger signals and provided the

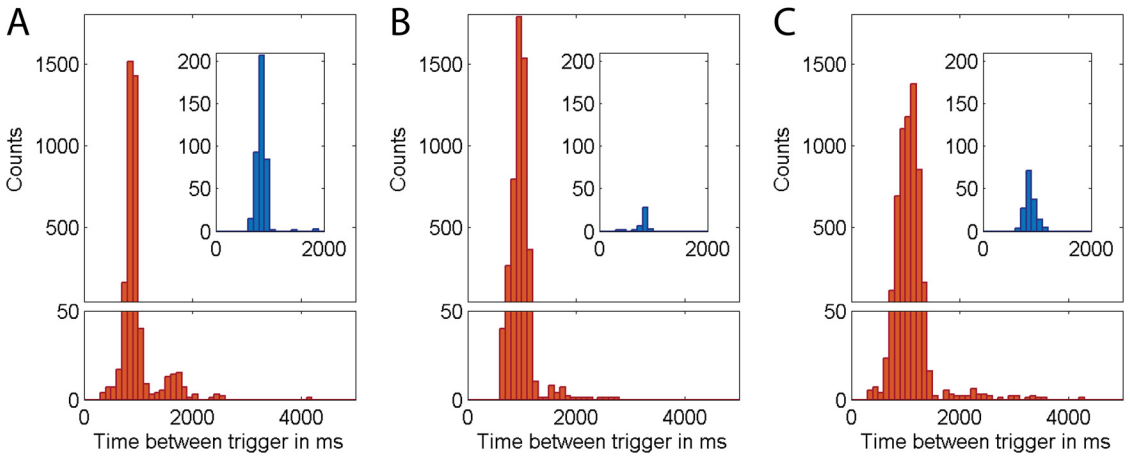

Figure 4. Histograms analyzing the apparent time interval between succeeding trigger events in 3 healthy subjects (A–C) outside (blue) and at the isocenter (red) of the magnet. The bins along the horizontal axis are separated by 100 milliseconds. For almost all events, the time elapsed with respect to the previous event is in the range of 1 RR-interval. Counts at considerably larger or shorter intervals indicate false negative and false positive triggering.

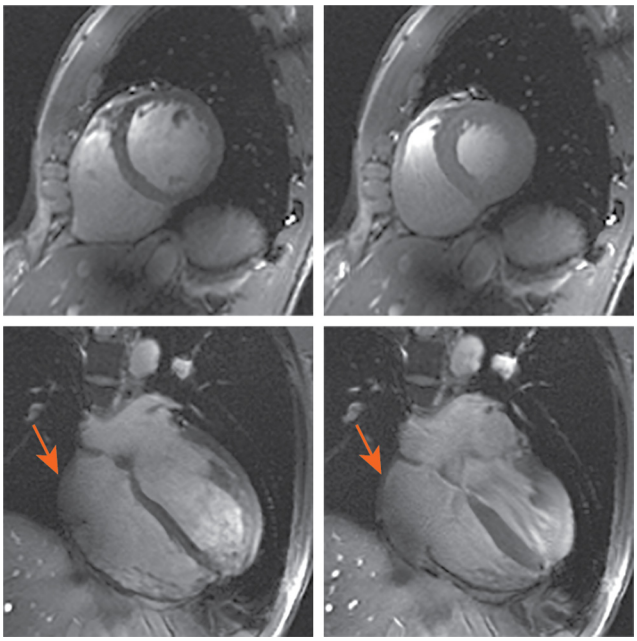

Figure 5. Images obtained using fully ECG-triggered cardiac cine imaging at ultra-high field. Shown are diastolic (left) and systolic (right) time frames of a short-axis (top) and horizontal long-axis (bottom) view. Myocardial walls are accurately delineated. Signal inhomogeneities induced by destructive B1 interferences are depicted (arrows).

basis for high-fidelity cardiac imaging. Despite severe ECG signal distortions due to the MHD effect and breathing motion, synchronized imaging was feasible without severe disruptions in all healthy volunteers. The attached pulse sensor was not required in any case as a substitute trigger device, and significant synchronization-related image artifacts were not observed.

In general, ECG signal distortions can be introduced by various motions and imaging gradients. In this initial study, the distorting effect of imaging gradients turned out to be small, although, as expected, considerable distortions were caused by the MHD effect. Particularly irregular and, in some cases, severe distortions could be attributed to breathing and subject motion. Even in presence of these adverse effects, the utilized trigger algorithm allows for an accurate R-wave detection, provided a learning phase in the absence of the magnetic field has been executed.

In the absence of the large magnetic field, ECG triggering was found to be highly accurate with the used setup. In the presence of the ultra-high field, the MHD effect led to significant distortion of the ECG signal time curves in all volunteers. Nevertheless, the overall synchronization accuracy remained high. As indicated by the histogram analysis, the length of almost all RR-intervals is within the range of a single RR-interval. The relatively high accuracy can be explained by the fact that the QRS complex of the ECG is typically only marginally impacted by the MHD effect, and the used trigger algorithm relies on real-time detection of the shape of the rising edge of the R-wave, rather than signal thresholding of the R-wave. In this way, the misplacement of trigger events and the generation of false positive events is minimized. Consequently, even in cases where the distorted T-wave of the ECG clearly exceeds the targeted R-wave, accurate cardiac synchronization is feasible.

The generally high trigger accuracy is also recognizable in the calculated vectorcardiograms. The location and the spread of the trigger events were not significantly affected by the exposure of the subject to the high magnetic field, despite the considerable increase in signal fluctuations. Inside and outside of the magnetic field, the VCG plots show different characteristic patterns. Although the pattern change itself is governed by the MHD effect, the additional dispersion of this pattern (Figure 2) can be attributed to the breathing motion and the associated movement of the chest with the electrodes through the static magnetic field. In this study, imaging gradients did not have a large influence on the VCG signal. As shown in Figures 2 and 3, they only caused tiny and high-frequency signal deflections.

To achieve high trigger accuracy at ultra-high field, careful subject preparation and electrode placement are essential to ensure good connection of the electrodes with the subject's skin and to achieve high input signals in all ECG channels. As depicted in Figures 2 and 3, gradient-induced ECG signal distortions can thus be kept small. A good preparation is particularly important for applications such as retro-gated cine CMR, where imaging gradients interfere with the QRS complex. Given the additional effect of breathing motion corrupting the ECG signal, properly instructing subjects on breathing techniques might be helpful in achieving accurate triggering. This is particularly the case for free-breathing imaging applications.

In this work, accurate ECG triggering was achieved by fully exploiting the technical capabilities of the ultra-high field scanner and trigger equipment. Apart from conducting an appropriate ECG learning phase, further hardware or software modifications were not required. Thus, the presented approach is widely available and ready to use. Recently, published studies indicate that using a larger number of ECG leads, the use of specifically tailored trigger algorithms or combinations of both can be advantageous in terms of trigger accuracy (36-40). Based on this, we assume that the use of more leads or further refinements of the algorithm could improve our results. However, the use of a large number of leads also adds to patient discomfort and preparation times.

Within the scope of this initial study, only a limited number of healthy subjects could be examined. Thus, it is important to note that the overall number of RR-intervals that could be analyzed outside of the magnet bore is rather low. Moreover, it is well-known that the success of ECG triggering can be highly subject-dependent, and certainly, a larger number of subjects need to be examined in future work to fully reveal the performance of the trigger technology at hand. Apart from that, ECG triggering can be particularly challenging in patient cohorts with cardiac arrhythmia, where the MHD effect can be more severe and variable.

In conclusion, we have shown that reliable cardiac ECG triggering is feasible in healthy volunteers at ultra-high

field by using a state-of-the-art 3-lead trigger device. The used trigger algorithm provided sufficient accuracy for high-fidelity cardiac cine imaging, despite severe ECG signal distortions due to the MHD effect. Future work will need to further evaluate the algorithm in larger cohorts and patients with cardiac arrhythmia. Apart from CMR, other ultra-high field imaging applications such as human brain functional MRI with physiological noise correction may benefit from the easy instrumentational setup and robust ECG triggering.

Supplemental Materials

Video 1: http://dx.doi.org/10.18383/j.tom.2016.00193.vid.01
Video 2: http://dx.doi.org/10.18383/j.tom.2016.00193.vid.02

ACKNOWLEDGMENTS

CHC would like to acknowledge funding by the University of Queensland Academic Title Holder Research Grant (ATHRF). The authors would like to thank Daniel Smith and Haris Haqqani (Cardiac Electrophysiology Unit, The Prince Charles Hospital, Brisbane, Queensland Australia) for their helpful advice on ECG devices, ECG triggering, and ECG electrode placement. The authors acknowledge the facilities of the National Imaging Facility (NIF) at the Centre for Advanced Imaging, University of Queensland, and support by the NIF fellow Steffen Bollmann.

Disclosures: KO and JR disclose being employed by Siemens Healthcare. JR holds a patent related to the work presented.

REFERENCES

1. Finn JP, Nael K, Deshpande V, Ratib O, Laub G. Cardiac MR imaging: state of the technology 1. Radiology. 2006;241(2):338–354.
2. Earls JP, Ho VB, Foo TK, Castillo E, Flamm SD. Cardiac MRI: recent progress and continued challenges. J Magn Reson Imaging. 2002;16(2):111–127.
3. Hundley WG, Bluemke DA, Finn JP, Flamm SD, Fogel MA, Friedrich MG, Ho VB, Jerosch-Herold M, Kramer CM, Manning WJ, Patel M, Pohost GM, Stillman AE, White RD, Woodard PK. ACCF/ACR/AHA/NASCI/SCMR 2010 expert consensus document on cardiovascular magnetic resonance. J Am Coll Cardiol. 2010; 55(23):2614–2662.
4. Wintersperger BJ, Reeder SB, Nikolaou K, Dietrich O, Huber A, Greiser A, Lanz T, Reiser MF, Schoenberg SO. Cardiac CINE MR imaging with a 32-channel cardiac coil and parallel imaging: impact of acceleration factors on image quality and volumetric accuracy. J Magn Reson Imaging. 2006;23(2): 222–227.
5. Schmitt M, Potthast A, Sosnovik DE, Polimeni JR, Wiggins GC, Triantafyllou C, Wald LL. A 128-channel receive-only cardiac coil for highly accelerated cardiac MRI at 3 Tesla. Magn Reson Med. 2008;59(6):1431–1439.
6. Stäb D, Ritter CO, Breuer FA, Weng AM, Hahn D, Köstler H. CAIPIRINHA accelerated SSFP imaging. Magn Reson Med. 2011;65(1):157–164.
7. Stäb D, Wech T, Breuer FA, Weng AM, Ritter CO, Hahn D, Köstler H. High resolution myocardial first-pass perfusion imaging with extended anatomic coverage. J Magn Reson Imaging. 2014;39(6):1575–1587.
8. Schmitter S, Moeller S, Wu X, Auerbach EJ, Metzger GJ, van de Moortele P-F, Uğurbil K. Simultaneous multislice imaging in dynamic cardiac MRI at 7T using parallel transmission. Magn Reson Med. 2016.
9. Manka R, Paetsch I, Schnackenburg B, Gebker R, Fleck E, Jahnke C. BOLD cardiovascular magnetic resonance at 3.0 tesla in myocardial ischemia. J Cardiovasc Magn Reson. 2010;12:54.
10. Zhang S, Uecker M, Voit D, Merboldt K-D, Frahm J. Real-time cardiovascular magnetic resonance at high temporal resolution: radial FLASH with nonlinear inverse reconstruction. J Cardiovasc Magn Reson. 2010;12:39.
11. Ohliger MA, Grant AK, Sodickson DK. Ultimate intrinsic signal-to-noise ratio for parallel MRI: electromagnetic field considerations. Magn Reson Med. 2003; 50(5):1018–1030.
12. Gutberlet M, Noeske R, Schwinge K, Freyhardt P, Felix R, Niendorf T. Comprehensive cardiac magnetic resonance imaging at 3.0 Tesla: feasibility and implications for clinical applications. Invest Radiol. 2006;41(2):154–167.
13. Snyder CJ, DelaBarre L, Metzger GJ, van de Moortele P-F, Akgun C, Ugurbil K, Vaughan JT. Initial results of cardiac imaging at 7 Tesla. Magn Reson Med. 2009;61(3):517–524.
14. van Elderen SGC, Versluis MJ, Westenberg JJ, Agarwal H, Smith NB, Stuber M, de Roos A, Webb AG. Right coronary MR angiography at 7 T: a direct quantitative and qualitative comparison with 3 T in young healthy volunteers. Radiology. 2010;257(1):254–259.
15. von Knobelsdorff-Brenkenhoff F, Tkachenko V, Winter L, Rieger J, Thalhammer C, Hezel F, Graessl A, Dieringer MA, Niendorf T, Schulz-Menger J. Assessment of the right ventricle with cardiovascular magnetic resonance at 7 Tesla. J Cardiovasc Magn Reson. 2013;15:23.
16. Graessl A, Renz W, Hezel F, Dieringer MA, Winter L, Oezerdem C, Rieger J, Kellman P, Santoro D, Lindel TD, Frauenrath T, Pfeiffer H, Niendorf T. Modular 32-channel transceiver coil array for cardiac MRI at 7.0T. Magn Reson Med. 2014;72(1):276–290.
17. Hezel F, Thalhammer C, Waiczies S, Schulz-Menger J, Niendorf T. High spatial resolution and temporally resolved T2* mapping of normal human myocardium at 7.0 tesla: an ultrahigh field magnetic resonance feasibility study. PLoS One. 2012;7(12).
18. Kober F, Jao T, Troalen T, Nayak KS. Myocardial arterial spin labeling. J Cardiovasc Magn Reson. 2016;18:22.
19. Clarke WT, Robson MD, Rodgers CT. Bloch-Siegert B1+-mapping for human cardiac (31) P-MRS at 7 Tesla. Magn Reson Med. 2015. doi: 10.1002/mrm. 26005 [Epub ahead of print].
20. Fischer SE, Wickline SA, Lorenz CH. Novel real-time R-wave detection algorithm based on the vectorcardiogram for accurate gated magnetic resonance acquisitions. Magn Reson Med. 1999;42(2):361–370.
21. Togawa T, Okai O, Oshima M. Observation of blood flow E.M.F. in externally applied strong magnetic field by surface electrodes. Med Biol Eng. 1967;5(2):169–170.
22. Krug JW, Rose G. Magnetohydrodynamic distortions of the ECG in different MR scanner configurations. In: 2011 Computing in Cardiology; 2011: pp. 769–772.
23. Jekic M, Dzwonczyk R, Ding S, Raman V, Simonetti O. Quantitative evaluation of magnetohydrodynamic effects on the electrocardiogram. In: 17th ISMRM Annual Meeting and Exhibition; 2009: p. 3795.
24. Tenforde TS. Magnetically induced electric fields and currents in the circulatory system. Prog Biophys Mol Biol. 2005;87(2–3):279–288.
25. Dietrich O, Reiser MF, Schoenberg SO. Artifacts in 3-T MRI: physical background and reduction strategies. Eur J Radiol. 2008;65(1):29–35.
26. Sievers B, Wiesner M, Kiria N, Speiser U, Schoen S, Strasser RH. Influence of the trigger technique on ventricular function measurements using 3-Tesla magnetic resonance imaging: comparison of ECG versus pulse wave triggering. Acta Radiol. 2011;52(4):385–392.
27. Suttie JJ, DelaBarre L, Pitcher A, van de Moortele PF, Dass S, Snyder CJ, Francis JM, Metzger GJ, Weale P, Ugurbil K, Neubauer S, Robson M, Vaughan T. 7 Tesla (T) human cardiovascular magnetic resonance imaging using FLASH and SSFP to assess cardiac function: validation against 1.5 T and 3 T. NMR Biomed. 2012;25(1):27–34.
28. Frauenrath T, Hezel F, Renz W, d'Orth Tde G, Dieringer M, von Knobelsdorff-Brenkenhoff F, Prothmann M, Menger JS, Niendorf T. Acoustic cardiac triggering: a practical solution for synchronization and gating of cardiovascular magnetic resonance at 7 Tesla. J Cardiovasc Magn Reson. 2010;12:67.
29. Krug J, Rose G, Stucht D, Clifford G, Oster J. Limitations of VCG based gating methods in ultra high field cardiac MRI. J Cardiovasc Magn Reson. 2013;15.
30. Kording F, Schoennagel B, Lund G, Ueberle F, Jung C, Adam G, Yamamura J. Doppler ultrasound compared with electrocardiogram and pulse oximetry cardiac triggering: a pilot study. Magn Reson Med. 2015;74(5):1257–1265.
31. Maderwald S, Orzada S, Lin Z, Schäfer LC, Bitz AK, Kraff O, Brote I, Häring L, Czylwik A, Zenge MO, Ladd SC, Ladd ME, Nassenstein K. 7 Tesla cardiac imaging with a phonocardiogram trigger device. In: 19th ISMRM Annual Meeting and Exhibition; 2011: p. 1322.
32. Brau AC, Brittain JH. Generalized self-navigated motion detection technique: preliminary investigation in abdominal imaging. Magn Reson Med. 2006;55(2): 263–270.
33. Buehrer M, Curcic J, Boesiger P, Kozerke S. Prospective self-gating for simultaneous compensation of cardiac and respiratory motion. Magn Reson Med. 2008; 60(3):683–690.

34. Larson AC, White RD, Laub G, McVeigh ER, Li D, Simonetti OP. Self-gated cardiac cine MRI. Magn Reson Med. 2004;51(1):93–102.
35. Schroeder L, Wetzl J, Maier A, Rehner R, Fenchel M, Speier P. A novel method for contact-free cardiac synchronization using the pilot tone navigator. In: 24th ISMRM Annual Meeting and Exhibition; 2016: p. 3103.
36. Odille F, Pasquier C, Abacherli R, Vuissoz PA, Zientara GP, Felblinger J. Noise cancellation signal processing method and computer system for improved real-time electrocardiogram artifact correction during MRI data acquisition. IEEE Trans Biomed Eng. 2007;54(4):630–640.
37. Krug JW, Rose GH, Stucht D, Clifford GD, Oster J. Filtering the magnetohydrodynamic effect from 12-lead ECG signals using independent component analysis. In: 2012 Computing in Cardiology; 2012:589–592.
38. Krug JW, Rose G, Clifford GD, Oster J. ECG-based gating in ultra high field cardiovascular magnetic resonance using an independent component analysis approach. J Cardiovasc Magn Reson. 2013;15:104.
39. Gregory TS, Schmidt EJ, Zhang SH, Ho Tse ZT. 3DQRS: a method to obtain reliable QRS complex detection within high field MRI using 12-lead electrocardiogram traces. Magn Reson Med. 2014;71(4):1374–1380.
40. Zhang SH, Tse ZT, Dumoulin CL, Kwong RY, Stevenson WG, Watkins R, Ward J, Wang W, Schmidt EJ. Gradient-induced voltages on 12-lead ECGs during high duty-cycle MRI sequences and a method for their removal considering linear and concomitant gradient terms. Magn Reson Med. 2016;75(5):2204–2216.
41. Frank M, Rößler J. Method for identifying an R-wave in an ECG signal, ECG measuring device and magnetic resonance scanner. US patent application 2010 0191134 A1. 29 July 2010.
42. Proakis JG. *Digital Communications*. 3rd ed. New York, NY: McGraw-Hill; 1995.
43. Knesewitsch T, Meierhofer C, Rieger H, Rößler J, Frank M, Martinoff S, Hess J, Stern H, Fratz S. Demonstration of value of optimizing ECG triggering for cardiovascular magnetic resonance in patients with congenital heart disease. J Cardiovasc Magn Reson. 2013;15(1):3.